IL NUOVO CIMENTO Vol. 27 C, N. 2 Marzo-Aprile 2004
DOI 10.1393/ncc/i2004-10016-0

Longitudinal spectra of wind velocity in the atmospheric surface layer perturbed by a small topographic ridge

F. Tampieri([1]), I. Mammarella([2]) and A. Maurizi([1])

([1]) *ISAC-CNR - Bologna, Italy*
([2]) *FMI - Helsinki, Finland*

(ricevuto l'11 Agosto 2004; approvato il 6 Settembre 2004)

Summary. — Turbulence measurements carried out in the near neutral surface layer are presented. The wind velocity components were measured with sonic anemometers at 2 and 10 m height. Three masts are considered, placed about 4 km upwind, on the top and about 6 km downwind of Inexpressible Island, a relief 300 m high and 1 km in cross-section. Spectral features are discussed in detail. Local equilibrium is found in the inertial subrange and in (at least in part of) the intermediate range, characterized by different slopes upwind and downwind (k^{-1} and $k^{-5/3}$, respectively) for the components parallel to the terrain.

PACS 92.60.Fm – Boundary layer structure and processes.

1. – Introduction

In many environmental applications, knowledge of atmospheric turbulence is often limited to the first two moments of velocity components. Steady and horizontally homogeneous conditions allow the use of the Monin-Obukhov Similarity Theory (MOST) to describe the surface layer structure. In this context, the spectral properties are expected to be completely defined, so that similarity spectra have been proposed in the literature and currently used.

Field observations and practical applications do not usually meet the steadiness and homogeneity conditions, and departures from the theory are commonly observed. Due to the number and complexity of the different phenomena affecting actual atmospheric boundary layers, a complete understanding still remains beyond reach. Our approach is to select situations in which specific departures from ideal conditions occur, in an attempt to make a first step towards understanding the complexity of the overall problem.

The purpose of this paper is to present and discuss measurements of longitudinal velocity spectra in the near neutral surface layer, in the presence of a small hump over a flat surface. The data are interpreted using similarity arguments, to suggest some generalization of the specific results.

2. – The similarity framework

In homogeneous and steady conditions, the energy spectrum tensor (the Fourier transform of the second order two-point, two-time velocity correlation tensor) is a function of the wavenumber vector and of frequency. This paper deals with time series of wind velocity components measured at fixed points; consistently, we shall present one-dimensional spectra, according to pp. 35 and 36 in [1], as a function of the (scalar) wavenumber $k = 2\pi\nu/U$ (where U is the mean wind velocity and ν the frequency), namely

$$E_i(k) = \frac{2}{\pi} U \int_0^\infty \overline{u_i(0)u_i(t)} \cos(2\pi\nu t) \mathrm{d}t \,, \tag{1}$$

where the frozen turbulence hypothesis is used. Attention is limited to the spectra of the diagonal terms of the Reynolds stress tensor.

In general, the similarity form of the spectrum may be written as

$$E_i(k) = \mathcal{U}_{(i)}^2 \mathcal{L}_{(i)} \Phi_{(i)} \left(k\mathcal{L}_{(i)}\right) \tag{2}$$

using a velocity scale $\mathcal{U}_{(i)}$ and a length scale $\mathcal{L}_{(i)}$, which may depend on i.

For instance, inertial subrange properties require that with sufficiently large wavenumbers k, for each component, it turns out that $\mathcal{U} \sim \varepsilon^{1/3}\mathcal{L}^{1/3}$ where ε the average energy dissipation rate and $\mathcal{L} \propto k^{-1}$ is the eddy size: thus the energy spectral density decays as $k^{-5/3}$.

At the other end of the spectrum, for $k = 0$, eq. (1) gives

$$E_i(0) = \frac{2}{\pi} \overline{u_i^2} L_i \,, \tag{3}$$

where L_i is the integral of the Eulerian time correlation function multipied by U, namely an estimate of the Eulerian integral length scale.

In the logarithmic near neutral surface layer the velocity scale for all the components is u_* constant with z, and $\varepsilon = u_*^3/\kappa z$ ($\kappa = 0.4$: the Von Kármán constant). Furthermore, at least for the vertical component, the integral length scale $L_3 = \kappa z$. According to [2] and to [3] the similarity form of the spectra in the near neutral surface layer may be written as

$$\frac{E_i(k)}{u_*^2 z} = \Phi_i(kz) \,, \qquad i = 1, 2, 3 \tag{4}$$

leading to the inertial subrange scaling (large-wavenumber scaling):

$$\Phi_i(kz) = C_{Ki}(kz)^{-5/3} \tag{5}$$

and to the small-wavenumber scaling

$$\Phi_i(kz) = \frac{2}{\pi} \frac{\overline{u_i^2}}{u_*^2} \left[1 + \mathcal{O}\left((kz)^2\right)\right] \,. \tag{6}$$

Thus the surface layer properties suggest that the same scaling must be correct for both the ends of the spectrum: for example, the widely known Kaimal spectrum [4]

is based on this observation. However, other situations can occur, suggesting different scalings.

Firstly, it must be noted that the integral length scale may not be a function only of the height z. For instance, in the stratified boundary layer, the Monin-Obukhov length L_{MO} is a relevant scale, as well as the wavelength if gravity waves are present. Zilitinkevich [5] suggested that the height of the boundary layer is to be accounted for to obtain a scale for the large wavelengths (eddies). Recent pipe flow data discussed by Morrison *et al.* [6] show that the small wavenumber part of the spectrum is affected by the pipe radius. In the bulk of the convective boundary layer, the eddies scale on the layer depth. In complex topography, the large scales are affected by the characteristic terrain scales.

Furthermore, the velocity variance normalized with the square of the friction velocity often shows a large variability. In a number of cases, the scale velocity is not expected to be strictly constant with height. For instance, Högström *et al.* [7] suggest that in shear boundary layers the variance of the vertical velocity varies as $\overline{u_3^2} \propto u_*^2(1+\beta z^{2/3})$. In the free convective sublayer, the vertical velocity variance grows as $z^{2/3}$. Downstream of an obstacle, experimental observations (see, for instance, the RUSHIL experiment [8]) show that the variances of all the velocity components have a maximum at the level of the hilltop.

According to these observations, the surface layer scaling eq. (4) is expected to fail in a number of cases, in the small-wavenumber range, where suitable velocity and length scales (different from friction velocity and distance from the ground) are necessary.

The transition between the inertial subrange and the small-wavenumber range also deserves some attention, as it contains signatures of peculiar dynamic effects.

At least for some components, a spectral range where the energy density does not depend on the length scale (in particular, on the distance from the ground) is expected. This is likely to be true for the components parallel to the ground in shear-dominated boundary layers ([9] and many others) as well as for the vertical velocity component in the convective boundary layer [10] (in this last case, at heights where buoyancy dominates over shear).

Thus extending the surface layer scaling, eq. (2) and eq. (4), we can write

$$E_i(k) = \mathcal{U}_i(z)^2 z \Phi_i(kz) \tag{7}$$

for a given k range. Under the condition $\partial E/\partial z = 0$, if the scale velocity changes as $z^{\gamma/2}$, it turns out that $\Phi \sim (kz)^{-\gamma-1}$. In the surface layer, where $\gamma = 0$, the spectrum slope is k^{-1}. This slope has been observed by many authors (see [11] for a review), and has stimulated different interpretations (see, *e.g.*, [12-16]). In the free convection layer, the scale velocity must be proportional to $w_* \sim z^{1/3}$, generating a $k^{-5/3}$ range (not to be confused with the inertial subrange). This range has been observed by [3].

3. – The field experiment

A field experiment was carried out during the Antarctic summer 1998-1999 in the Terra Nova Bay region. In this area, strong katabatic winds blowing from the Reeves Glacier produce surface layers characterised by long periods of almost neutral steady conditions. A mast equipped with two sonic anemometers at 2 m and 10 m was located in the nearly flat and iced area called Nansen Ice Sheet (NIS), 14 km downstream of the

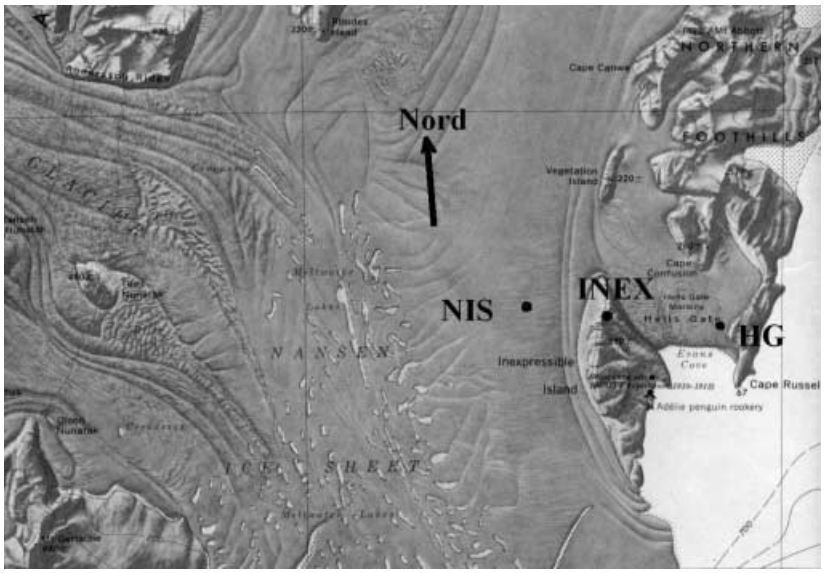

Fig. 1. – Map of the experimental site.

foot of the Reeves Glacier. A second mast 2 m high was placed at the top of Inexpressible Island (INEX), a steep obstacle of height $H = 300$ m, where bare rock at the ground produces a large surface roughness. Further information on the experimental site and flow characteristics can be found in Mammarella *et al.* [17], who provide also some details on the data treatment. A third mast 10 m high was located in Hell's Gate (HG), the flat area about 6 km downstream of the obstacle. The locations of the masts are reported in fig. 1.

The data were sampled at 20.8 Hz for NIS and INEX, and at 10 Hz for HG site; standard rotation and filtering to eliminate spikes were performed. Each data set covers 52 min. The data sets were selected in order to have almost steady situations, with a logarithmic near neutral surface layer (the components of the Reynolds stress tensor $\overline{u_i u_j}, i, j = 1, 2, 3$ do not change by more than 0.05 percent between 2 and 10 m), and airflow broadly aligned from NIS to HG, impinging to the obstacle normally to the watershed. In such conditions, the mean wind velocity is $U > 10$ m/s at 10 m (corresponding to $U > 8$ m/s at 2 m) and the mean wind direction is in the range 260°–285°.

4. – Upwind, flat terrain spectra

The spectra measured at NIS site are presented in fig. 2, normalized according to the large-wavenumber scaling, eq. (4). Single cases are reported, with different symbols.

E_1 shows both the $k^{-5/3}$ and the k^{-1} ranges, where all the spectra collapse fairly well; E_2 is similar, but the k^{-1} range is less defined and presents a larger scatter; E_3 shows the $k^{-5/3}$ range and an extended transition towards the k^0 range. Thus, the high wavenumber scaling is verified; the $k^{-5/3}$ range occurs for $kz > 1$ for E_1 and for slightly larger value for E_3.

For all the spectra, the scatter of data is large at small wavenumbers. The velocity components standard deviations do not scale well with u_*, and show a large variability (fig. 3).

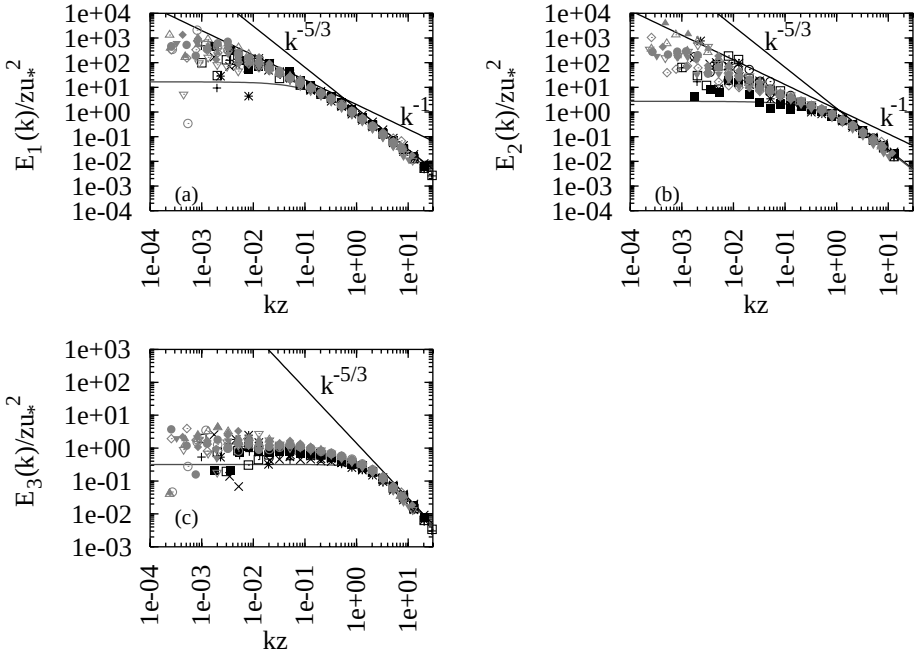

Fig. 2. – Spectra measured at NIS at 2 m and 10 m for the longitudinal (a), lateral (b) and vertical (c) components. The lines show the reference spectra [4].

Similarly, the scales L_i computed by integrating the correlation function appear quite scattered. Broadly speaking, $L_1(z = 10\,\mathrm{m})/L_1(z = 2\,\mathrm{m}) \simeq 1.7$, whereas the same ratio for the vertical scales is quite variable, without any representative value (considerations from MOST would suggest 5, of course). These observations support the need for a small-wavenumber scaling, based on the large-scale structure of the surface layer turbulence, consistent with eq. (2), rather than eq. (6). Scaling the spectra with $\overline{u_i^2}$ and L_i leads to a good collapse of the data for $i = 1$, but not for $i = 3$: this suggests that the large variability of L_3 is a signature of undetected influences on the large scales.

To give an objective estimate of the existence and extension of the different ranges and to evaluate the constants characterizing the spectra, spectra E_1 and E_3 have been fitted with a schematic model, as follows:

$$E_i(k) = A_i, \qquad k < K_{\Lambda i}\,, \tag{8}$$

$$E_i(k) = B_i k^{-1-\gamma_i}, \qquad K_{\Lambda i} \le k < K_{Ki}\,, \tag{9}$$

$$E_i(k) = C_i k^{-5/3}, \qquad k \ge K_{Ki}\,, \tag{10}$$

where $i = 1, 3$ and $\gamma_1 = 1$, whereas γ_3 is to be determined by the fit. This simple model allows a partitioning the spectrum into the large-wavenumber and small-wavenumber ranges, with a transition in between. Coefficients are fixed by matching the three ranges,

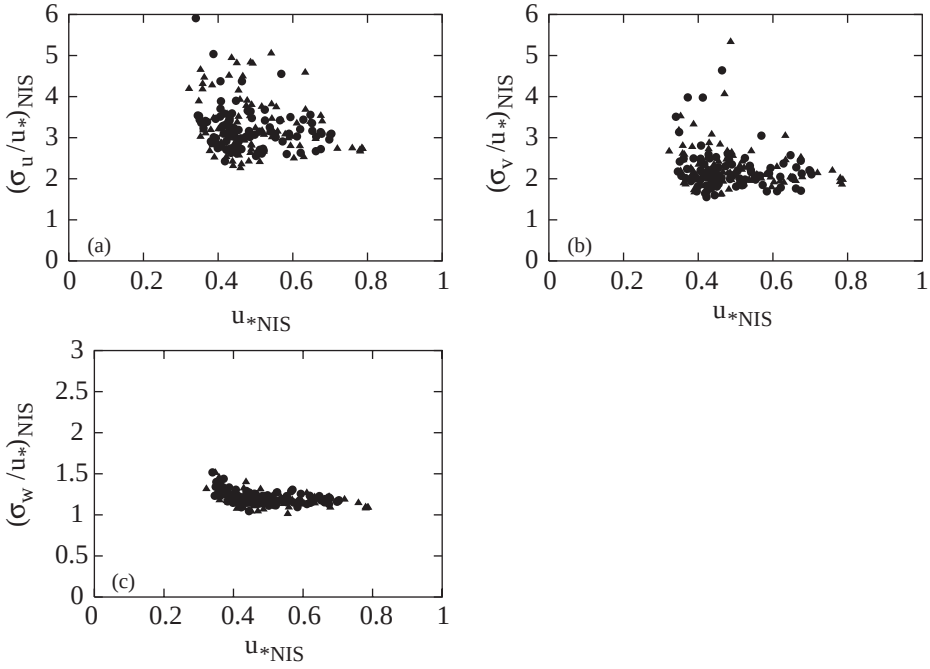

Fig. 3. – Normalised standard deviations of velocity fluctuation $\sigma_i/u_* \equiv \left(\overline{u_i^2}\right)^{1/2}/u_*$ as a function of u_* for the longitudinal (a), lateral (b) and vertical (c) component, measured at 2 m (•) and 10 m (▲) at NIS site.

so that

$$A_i = C_i K_{Ki}^{-5/3} \left(\frac{K_{Ki}}{K_{\Lambda i}}\right)^{1+\gamma_i} , \tag{11}$$

$$B_i = C_i K_{Ki}^{\gamma_i - 2/3} \tag{12}$$

and, from eq. (5),

$$C_i = C_{Ki} u_*^2 z^{-2/3} . \tag{13}$$

The model depends on the three parameters C_{Ki}, K_{Ki}, $K_{\Lambda i}$ for $i = 1$, and on four parameters (also on γ_3) for $i = 3$. Their values are estimated by minimising the function

$$F_i(\ln C_{Ki}, \ln K_{Ki}, \ln K_{\Lambda i}, \ln \gamma_i) = \sum_{m=1}^{n} \frac{1}{(\ln \epsilon_{im})^2} (\ln E_i(k_m) - \ln E_{im})^2 , \tag{14}$$

where E_{im} are the i-component experimental data and ϵ_{im} are their associated errors (estimated as the inverse of the standard deviation). The minimization numerical algorithm used is based on a quasi-Newton method (IMSL).

TABLE I. – *Model parameters for the longitudinal spectrum E_1. In brackets the standard deviations are reported.*

	$K_{\Lambda 1}(\mathrm{m}^{-1})$	$K_{K1}(\mathrm{m}^{-1})$	C_{K1}	$\log(K_{K1}/K_{\Lambda 1})$
10 m	$1.8 \cdot 10^{-3}$ $(1.4 \cdot 10^{-3})$	$7.0 \cdot 10^{-2}$ $(2.0 \cdot 10^{-2})$	0.47 (0.07)	1.7 (0.3)
2 m	$2.3 \cdot 10^{-3}$ $(1.7 \cdot 10^{-3})$	0.23 (0.05)	0.41 (0.08)	2.1 (0.2)
β-Student	0.5	$5 \cdot 10^{-8}$	0.1	0.02

The fitted values of the model parameters are reported in tables I and II. The Student's t-test is used to evaluate the significance of the difference between the parameter values at 2 m and 10 m. A small numerical value of β (say $\beta < 0.01$) means that the observed difference is significant.

Basically, this quantitative analysis confirms the observations made above, as well as providing further quantitative information. As far as E_1 is concerned, the lower limit for the inertial subrange is proportional to the height: namely, $zK_{K1} = 0.6 \pm 0.2$. The value of $C_{K1} \sim 0.4$–0.5 is approximately constant for the entire data set: for the purpose of comparison, note that [3] reported $C_{K1} = 0.51$ from the atmospheric neutral data at Tsimlyank, and $C_{K1} = 0.48$ from laboratory data. The large scales are characterised by $K_{\Lambda 1}$, which is scattered around a value independent of height.

In the case of E_3, the fit justifies the existence of an intermediate region with exponent $\gamma_3 \simeq 0.5$ for $zK_{z3} < 2.5$. $C_{K3} \simeq 0.6$ is fairly constant and compares well with [3], who reported $C_{K3} = 0.65$ for the Tsimlyank data. The scale length does not scale with height, leading to $zK_{K3} \sim 2$–4.

To assess the significance of the intermediate range, the value of $\log(K_{zi}/K_{\Lambda i})$ must be considered. From the fit, it results that the intermediate range extends for more than one decade. Moreover, it decreases with z, in accordance with the findings of [7], where only K_{Ki} decreases with height, while $K_{\Lambda i}$ is not affected or only weakly affected by the distance from the wall.

TABLE II. – *As in table I for E_3.*

	$K_{\Lambda 3}(\mathrm{m}^{-1})$	$K_{K3}(\mathrm{m}^{-1})$	C_{K3}	γ_3	$\log(K_{K3}/K_{\Lambda 3})$
10 m	0.03 (0.02)	0.4 (0.1)	0.6 (0.1)	0.6 (0.1)	1.2 (0.3)
2 m	0.04 (0.02)	1.0 (0.1)	0.6 (0.1)	0.45 (0.07)	1.5 (0.2)
β-Student	0.5	$3 \cdot 10^{-9}$	0.9	$4 \cdot 10^{-2}$	$1. \cdot 10^{-2}$

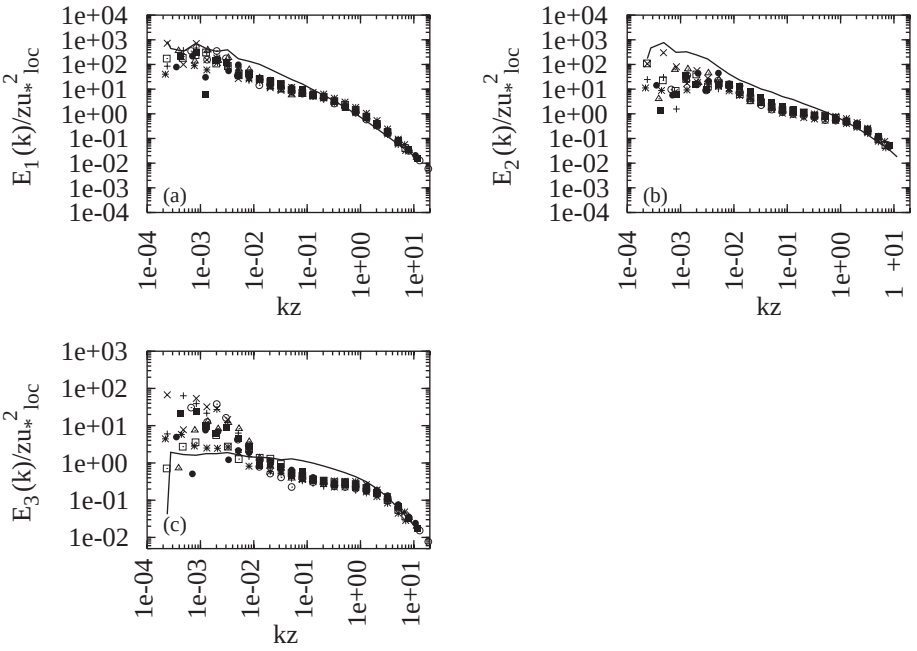

Fig. 4. – Single spectra measured at 2 m at the top of INEX for the longitudinal (a), lateral (b) and vertical (c) component, normalised with local u_* values. The solid lines represent the NIS-averaged spectra.

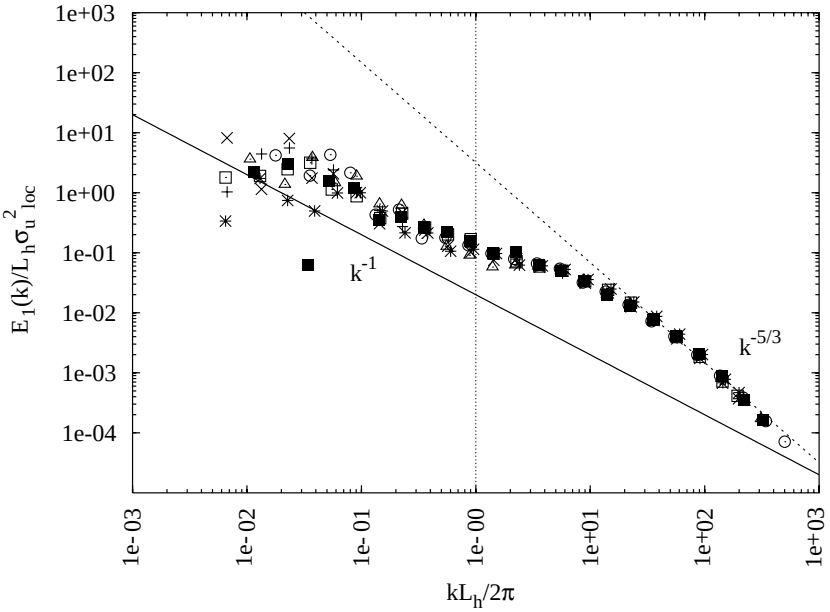

Fig. 5. – Longitudinal velocity spectra, measured on INEX, normalised with the local variances and with the effective scale of topography.

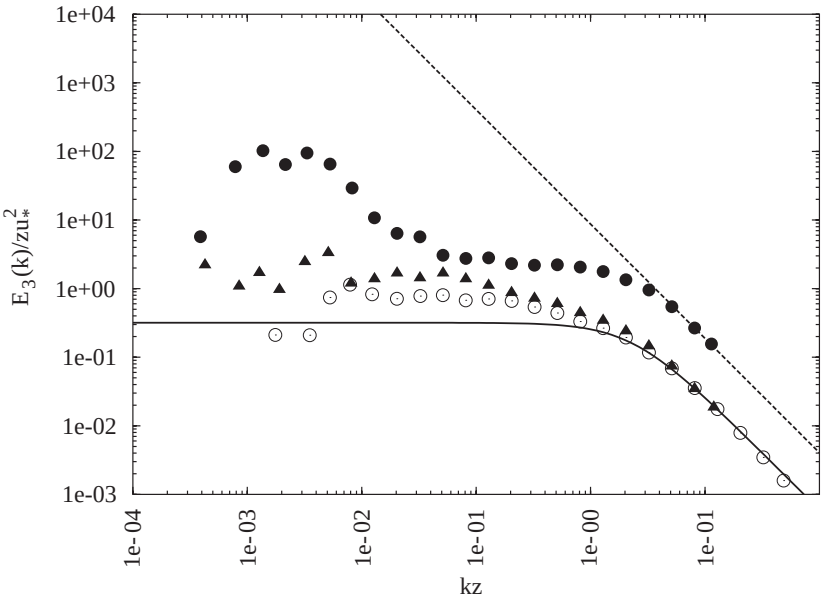

Fig. 6. – Example of a single spectrum (13-12-1998 h 10.30) of the vertical component, measured upwind at 2 (▲) and 10 m (○), and on the INEX top at 2 m (●), normalised with the upwind u_* value. The dashed line is obtained from eq. (15).

5. – Spectra at the top of the obstacle

Average spectra measured at 2 meters on the top of the obstacle have been discussed elsewhere [18]. The single spectra normalized according to eq. (4) are plotted in fig. 4. This scaling produces a good collapse of data in the high wavenumber range, showing that (local) equilibrium occurs for that range.

The increase of the lower limit of the $k^{-5/3}$ range is consistent with the shear-limited scale length formulation by [19], both for the vertical and horizontal components.

It is worth noting that a limited k^{-1} range appears for E_1, supporting the idea that this range is an extension of the inertial subrange at scales where the influence of the wall induces anisotropy in the turbulence structure.

Larger scales are affected by the forcing due to the obstacle. This leads to a characteristic change of slope at $kL_h = \mathcal{O}(1)$, with L_h being the effective horizontal scale of topography (fig. 5). For effective scale, we mean a measure of the overall extension of the topography plus the almost stagnant separated bubble upstream; it has been estimated so that H/L_h is equal to the mean slope of the streamlines measured at the top of the obstacle.

In fig. 6 a single case is analyzed, in order to compare upstream and hilltop conditions. It shows the increase in kinetic energy density in the inertial subrange due to the increase of shear, which in turn increases the friction velocity at hilltop:

$$E_3^{(\mathrm{INEX})}(k) \simeq \left(\frac{u_*^{(\mathrm{INEX})}}{u_*^{(\mathrm{NIS})}} \right)^2 E_3^{(\mathrm{NIS})}(k), \qquad kz > 1\,. \tag{15}$$

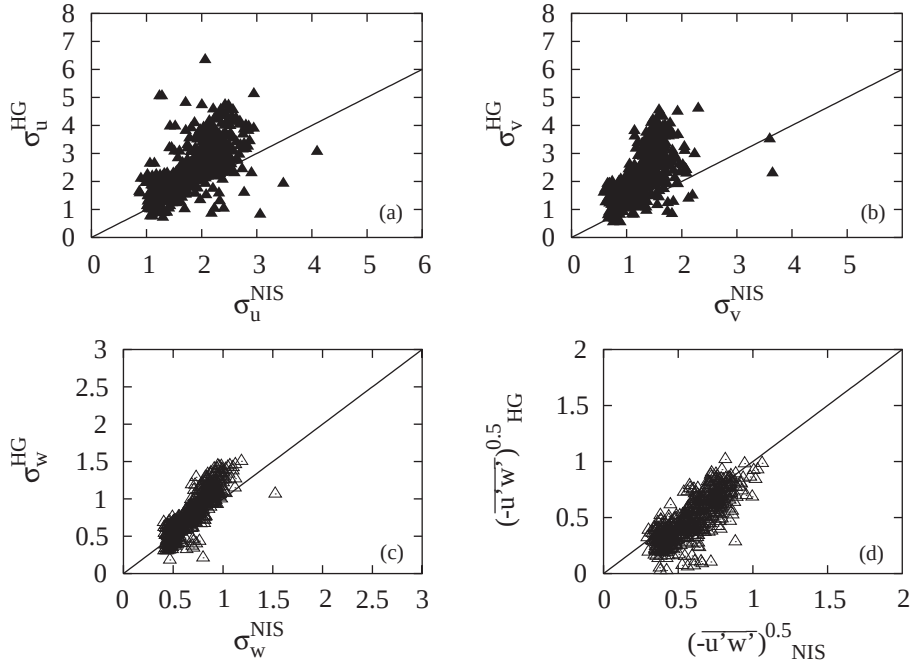

Fig. 7. – Scatter plots between the root square of NIS and HG turbulent stress values for the longitudinal (a), lateral (b), vertical (c) component and $\overline{u'w'}$ (d).

It is also possible to note the decrease in the scale K_{K3}^{-1} due to the shear limitation to the eddy scale.

6. – Spectra in the lee of the obstacle

Turbulence in the lee of the obstacle is affected by the wake, so that even if the mast is placed on flat terrain, advection is expected to be important in producing departures from standard similarity results. In fig. 7 the square root of the Reynolds stresses measured at HG is plotted as a function of the corresponding value at NIS (both at 10 m). Typically the diagonal terms are higher downstream, while the $\overline{u'w'}$ term is not. We can infer that the turbulent energy advection is larger than local shear production.

Energy spectra are reported in fig. 8 according to the large-wavenumber scaling. The averaged NIS 10 m high spectra are also reported for comparison. Local equilibrium is verified in the inertial subrange, $kz > 1$, where a clear $k^{-5/3}$ slope appears. It is worth noting that a similar slope appears approximately in the range $0.03 < kz < 1$, for the horizontal velocity components, while the vertical one does not greatly depart from the NIS case. As observed above, this slope could be explained by the modification of the z-independent range (the k^{-1} range) as the scale velocity varies (increasing) with height. Consistently, this feature occurs for the components of the velocity parallel to the ground.

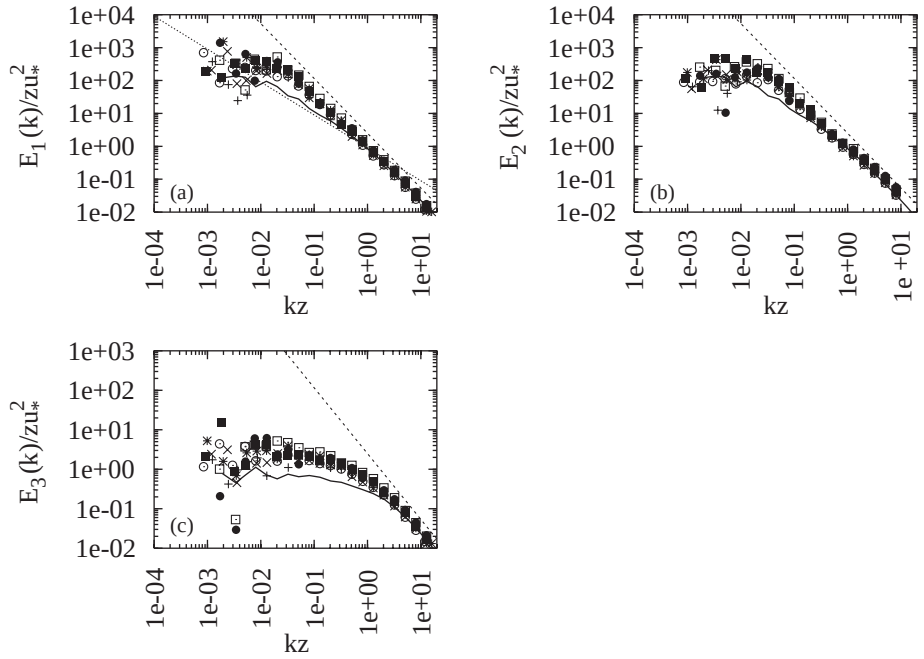

Fig. 8. – Single HG spectra measured at 10 m for the longitudinal (a), lateral (b) and vertical (c) component, normalised with NIS u_* values. The solid lines represent the NIS averaged spectra, while the dashed and dotted lines represent the $k^{-5/3}$ and k^{-1} slopes, respectively.

7. – Conclusions

The main result of the analysis concerns the existence of the k^{-1} range for spectral densities, which is confirmed as far as the horizontal components of the velocity are concerned. Conversely, there is no evidence of such a range in the case of the vertical component.

Moreover, local equilibria are found at least in the inertial subrange, even in sites where the effects of inhomogeneity on the overall turbulent flow are strong.

Going into greater detail for the vertical component, the inertial subrange is found for $zK_{z3} > 3 \pm 1$, or for length scale $L_3 \simeq z/3$. This is broadly consistent (although flawed by the wide scatter) with the classical result $L_3 = \kappa z$, as are the values of the constants C_{Ki} (in particular, C_{K3}/Ck_{K1} follows quite closely the 4/3 isotropy relation).

For $E_1(k)$ the normalized lower limit zK_{K1} of the inertial subrange is less than 1, suggesting that the length-scale at which the spectral energy is influenced by the ground is a little larger than z. This subrange is present at all three sites: it means that local equilibrium is attained in the surface layer, even in this wavenumber interval (wavenumbers smaller than those of the inertial subrange).

The inertial subrange extends towards the smaller wavelengths only for the spectra of velocity components parallel to ground. The slope is k^{-1} for unperturbed flat terrain data and $k^{-5/3}$ for data in the lee of the obstacle. The width of this range is typically more than a decade. It is reduced in the spectra over the top, as the influence of the topography-induced perturbations becomes significant.

The small-wavenumber range is less understood, because the data produce a large scatter, and the large-scale forcings affecting the spectra are beyond the reach of quantitative evaluation.

* * *

This work has been carried out in the framework of the Italian National Programme for Research in Antarctica (PNRA). The authors would like to thank A. M. Sempreviva for providing the HG raw data set.

REFERENCES

[1] Batchelor G. K., *The Theory of Homogeneous Turbulence*, 1970th ed. (Cambridge University Press) 1953.
[2] Monin A. S. and Yaglom A. M., *Statistical Fluid Mechanics*, Vol. II (MIT Press, Cambridge) 1975.
[3] Kader B. A. and Yaglom A. M., *Spectra and correlation functions of surface layer turbulence in unstable thermal stratification*, in *Turbulence and Coherent Structures*, edited by Metais O. and Lesieur M. (Kluwer Academic Press, Dordrecht) 1991.
[4] Kaimal J. C., Wyngaard J. C., Izumi Y. and Coté O. R., *Q. J. R. Meteorol. Soc.*, **98** (1972) 563.
[5] Zilitinkevich S. S., *Izv. Akad. Nauk SSSR*, **7** (1971) 1263.
[6] Morrison J. F., Jiang W., McKeon B. J. and Smits A. J., *Phys. Rev. Lett.*, **88** (2002) 214501.
[7] Högström U., Hunt J. C. R. and Smedman A., *Boundary-Layer Meteorol.*, **103** (2002) 101.
[8] Khurshudyan L. H., Snyder W. H. and Nekrasov I. V., *Flow and Dispersion of Pollutants over Two-Dimensional Hills: Summary Report on Joint Soviet-American Study*, Tech. Rep. EPA-600/4-81-067, res. Tri. Pk., NC (1981).
[9] Hunt J. C. R. and Morrison J. F., *Eur. J. Mech. B - Fluids*, **19** (2000) 673.
[10] Alberghi S., Maurizi A. and Tampieri F., *J. Appl. Meteorol.*, **41** (2002) 885.
[11] Katul G. and Chu C. R., *Boundary-Layer Meteorol.*, **86** (1998) 279.
[12] Tchen C. M., *J. Res. National Bureau of Standards*, **50** (1953) 51.
[13] Olla P., *Phys. Rev. E*, **57**, (1998) 2824.
[14] Nikora V., *Phys. Rev. Lett.*, **83** (1999) 734.
[15] Hunt J. C. R. and Carlotti P., *Flow, Turbulence and Combustion*, **66** (2001) 453.
[16] Drobinski P., Carlotti P., Newson R. K., Banta R. M., Foster R. C. and Redelsperger J., *J. Atmos. Sci.*, **61** (2004) 699.
[17] Mammarella I., Tampieri F., Nardino M. and Tagliazucca M., to be published in *Environmental Fluid Mechanics*.
[18] Tampieri F., I. Mammarella and A. Maurizi, *Boundary-Layer Meteorol.*, **109** (2003) 85.
[19] Hunt J. C. R., Moin P., Lee M., Moser R. D., Spalart P., Mansour N. N., Kaimal J. C. and Gaynor E., *Cross correlation and length scales in turbulent flows near surfaces*, in *Advances in Turbulence 2*, edited by Fernholz H.-H. and Fiedler H. (Springer-Verlag) 1989.